

Note: This is a draft of a paper submitted for publication. Contents of this paper should not be quoted or referred to without permission of the author(s).

To be presented as an invited paper at the  
*European Materials Research Society 2003 Spring Meeting*  
Strasbourg, France  
June 10-13, 2003

## **Generalized Ellipsometry for Materials Characterization**

G. E. Jellison, Jr.

Condensed Matter Sciences Division  
Oak Ridge National Laboratory  
Oak Ridge, TN 37831-6030

Submitted June 2003

The submitted manuscript has been authored by a contractor of the U.S. Government under contract No. DE-AC05-00OR22725. Accordingly, the U.S. Government retains a nonexclusive, royalty-free license to publish or reproduce the published form of this contribution, or allow others to do so, for U.S. Government purposes."

Prepared by the  
CONDENSED MATTER SCIENCES DIVISION  
OAK RIDGE NATIONAL LABORATORY  
Managed by  
UT-BATTELLE, LLC, for the  
U.S. DEPARTMENT OF ENERGY  
Under Contract No. DE-AC05-00OR22725

# Generalized Ellipsometry for Materials

## Characterization

G. E. Jellison, Jr.

Condensed Matter Sciences Division

Oak Ridge National Laboratory

Oak Ridge, TN 37831-6030

### Abstract

Ellipsometry experiments normally measure 2-4 parameters, which are converted to the ellipsometric parameters  $\psi$  and  $\Delta$ . This is usually sufficient for many samples, but more complicated situations (such as anisotropic or depolarizing samples) require more sophisticated measurements.

Over the last 7 years, we have developed the two-modulator generalized ellipsometer (2-MGE), which measures 8 elements of the sample Mueller matrix simultaneously either in reflection or transmission. In reflection, the 2-MGE totally characterizes light reflection from anisotropic samples, measuring the normal ellipsometry parameters, as

well as the cross-polarization and depolarization effects. Applications include the determination of the spectroscopic optical functions of uniaxial materials (such as  $\text{TiO}_2$  and  $\text{ZnO}$ ), and the measurement of cross-polarization from diffractive structures. In transmission, the 2-MGE completely characterizes a general linear diattenuator and retarder. Applications include the measurement of the retardation and diattenuation of film polarizers and internal electric fields in  $\text{LiNbO}_3$  and  $\text{CdZnTe}$  under bias.

## 1. Introduction

Optical measurements that conserve the wavelength (thus eliminating such processes as Raman scattering and photoluminescence) can generally be divided into three categories, depending on the complexity of the measurement.

1. Reflection and transmission measurements. These measurements determine the fraction of light intensity that is lost when the incident light beam is transmitted through or is reflected from the front surface of a sample. The accuracy of this type of measurement suffers from scattering losses and requires a very linear detector. In addition, reflection and transmission measurements are not sensitive to small phase shifts.

2. Normal ellipsometry measurements. These experiments are polarization-sensitive, and determine ratios of certain characteristics of the reflected or transmitted light for s- and p-polarized light. Traditionally, one measures characteristics of the reflection (or transmission) ratio:

$$\rho = \frac{r_p}{r_s} = \tan(\psi)e^{i\Delta} \quad (1)$$

where  $r_p$  ( $r_s$ ) is the complex reflection ratio for light polarized parallel (perpendicular) to the plane of incidence. The angles  $\psi$  and  $\Delta$  are the traditional ellipsometry parameters, and are the naturally measured quantities in a nulling ellipsometry measurement. Modern spectroscopic ellipsometers measure 2 to 4 independent parameters. However, these parameters<sup>1</sup> are usually not  $\psi$  and  $\Delta$  directly, but rather elements of the sample Mueller

matrix, which are trigonometric functions of  $\psi$  and  $\Delta$ . As a result, normal ellipsometry measurements are usually not capable of measuring characteristics of very complicated samples that may contain depolarization or cross-polarization.

3. Generalized ellipsometry measurements. These experiments<sup>2-6</sup> are similar to the normal ellipsometry experiments, but determine 8 to 15 elements of the sample Mueller matrix. Because of the complexity of the measurements, these experiments can deal with considerably more complicated situations, including depolarization, cross polarization in reflection measurements, and rotated diattenuators and retarders in transmission.

In this paper, we will review the capabilities of reflection and transmission generalized ellipsometry as performed by the two-modulator generalized ellipsometer (2-MGE), as described in refs. 2. Although this instrument measures only 8 of the 15 elements of the reduced sample Mueller matrix in each configuration, this is sufficient for a large number of experimental situations. In addition, 2-MGE measurements require no physical rotation of an optical element during measurement, making registration very accurate: all measured parameters are taken at exactly the same point of the sample.

## **2. Description of the 2-MGE**

The 2-MGE system used for transmission ellipsometry measurements is described in detail in refs. 2 and 7. Briefly, it consists of two polarizer-photoelastic modulator (PEM) pairs, each operating at a different resonant frequency. One polarizer-PEM pair is used as the polarization state generator (PSG) on the input arm of the ellipsometer, while the other is used as the polarization state analyzer (PSA) on the output arm of the ellipsometer. The two PEMs are resonant devices that are cut to oscillate at different

frequencies (~50 and ~60 kHz in our case). Typically, the PEM operates with a Q in excess of 10,000, making it a very stable device with respect to frequency variation. The polarizers are oriented at 45° with respect to the major oscillation axis of PEMs.

The light intensity reaching the detector in any 2-MGE is a very complicated function of time, but can be expressed as<sup>2</sup>

$$\begin{aligned} \text{Intensity}(t) = & I_{dc} + I_{X0} X0 + I_{Y0} Y0 + I_{X1} X1 + I_{Y1} Y1 + I_{X0X1} X0 X1 + I_{X0Y1} X0 Y1 + \\ & I_{Y0X1} Y0 X1 + I_{Y0Y1} Y0 Y1. \end{aligned} \quad (2a)$$

The terms  $I_{dc}$ ,  $I_{X0}$ ,  $I_{Y0}$ , etc. are constants that multiply the basis functions:

$$X0 = \sin(A_0 \sin(\omega_0 t)), \quad (2b)$$

$$Y0 = \cos(A_0 \sin(\omega_0 t)), \quad (2c)$$

$$X1 = \sin(A_1 \sin(\omega_1 t)), \quad (2d)$$

$$Y1 = \cos(A_1 \sin(\omega_1 t)). \quad (2e)$$

These basis functions are not just Fourier basis functions, but rather sines and cosines of sines. The modulator amplitudes ( $A_0$  and  $A_1$ ) are measured in angular units (usually radians) and the modulator frequencies are given by  $\omega_0$  and  $\omega_1$ .

The information content of the data from the 2-MGE is contained in the 8 parameters  $I_{X0}$ ,  $I_{Y0}$ , etc. which can be easily normalized to the dc light intensity  $I_{dc}$ . These 8 parameters are then related directly to elements of the sample Mueller matrix, depending only upon the azimuthal angles of PSG and the PSA. The sample Mueller matrix is

represented by For example, if the PSG and PSA are oriented at  $(0^\circ, 45^\circ)$  with respect to the primary reference frame, the sample Mueller matrix is represented by

$$\mathbf{M} = \begin{bmatrix} 1 & \bullet & -I_{Y0} & I_{X0} \\ I_{Y1} & \bullet & -I_{Y0Y1} & I_{X0Y1} \\ \bullet & \bullet & \bullet & \bullet \\ -I_{X1} & \bullet & I_{Y0X1} & -I_{X0X1} \end{bmatrix}, \quad (3)$$

The dots in the matrices of Eq. 3 represent unmeasured quantities in that configuration, and the coefficient of the intensity waveform is placed at the Mueller matrix position of the measured element. By combining the results of these this configuration and the configuration where the PSG and PSA are oriented at  $(0^\circ, 45^\circ)$  with respect to the primary reference frame, then only the  $m_{22}$  and  $m_{33}$  components remain unmeasured.

## 2.1 2-MGE in Reflection

The above analysis is valid for the 2-MGE whether it is aligned in the reflection mode (normal ellipsometry configuration) or in the transmission mode. If the sample is isotropic in the reflection mode, allowing for simple depolarization, then the sample Mueller matrix is given by<sup>8</sup>

$$M = \begin{bmatrix} 1 & -\beta N & 0 & 0 \\ -\beta N & \beta & 0 & 0 \\ 0 & 0 & \beta C & \beta S \\ 0 & 0 & -\beta S & \beta C \end{bmatrix} \quad (4a)$$

where

$$N = \cos(2\psi) \quad (4b)$$

$$S = \sin(2\psi) \sin(\Delta) \quad (4c)$$

$$C = \sin(2\psi) \cos(\Delta) \quad (4d)$$

and  $\beta$  is the fraction of polarized light after the sample, called the polarization factor;  $\beta = 1$  for no depolarization. If the Mueller matrix elements  $m_{21}$ ,  $m_{43}$ , and  $m_{44}$  are measured, then

$$(m_{21}^2 + m_{43}^2 + m_{44}^2) = \beta^2, \quad (4e)$$

thus measuring the polarization factor. Note that the elements of the sample Mueller matrix can only be reduced to the  $\psi \Delta$  representation if there is no depolarization. If there is no depolarization, then equation 1 becomes

$$\rho = \frac{r_p}{r_s} = \tan(\psi) e^{i\Delta} = \frac{C + iS}{1 + N} \quad (4f)$$

For anisotropic samples in the reflection mode, the s- and p- polarizations are no longer eigenmodes of reflection. That is, some of the incoming s-polarized light can be converted to p-polarized light, and visa versa. These are expressed in terms of the cross polarization reflection coefficients  $r_{sp}$  and  $r_{ps}$ . If there is no depolarization, then the ellipsometric data can be expressed in either the  $\psi \Delta$  representation, the  $\rho$  representation, or the NSC representation:

$$\rho = \frac{r_{pp}}{r_{ss}} = \tan(\psi) e^{i\Delta} = \frac{C + iS}{1 + N} \quad (5a)$$

$$\rho_{ps} = \frac{r_{ps}}{r_{ss}} = \tan(\psi_{ps})e^{i\Delta_{ps}} = \frac{C_{ps} + iS_{ps}}{1 + N} \quad (5b)$$

$$\rho_{sp} = \frac{r_{sp}}{r_{ss}} = \tan(\psi_{sp})e^{i\Delta_{sp}} = \frac{C_{sp} + iS_{sp}}{1 + N} \quad (5c)$$

If the sample does partially depolarize the light, then the NSC representation must be used, and the depolarization factor  $\beta$  can be determined.<sup>1,2</sup>

## 2.2 2-MGE in Transmission

In transmission for a linear diattenuator and retarder with no depolarization, the sample Mueller matrix is similar to that of the reflection Mueller matrix, but the meaning of the N, S, and C coefficients is considerably different. One additional degree of freedom for transmission measurements is that it is trivial to change the direction of the principal axis of the sample with respect to the reference frame of the instrument by simply rotating it. In this case, the sample Mueller matrix is given by

$$\mathbf{M} = \begin{bmatrix} 1 & -C_s N & -S_s N & 0 \\ -C_s N & C_s^2 + S_s^2 C & C_s S_s (1 - C) & -S_s S \\ -S_s N & C_s S_s (1 - C) & C_s^2 + S_s^2 C & C_s S \\ 0 & S_s S & -C_s S & C \end{bmatrix}, \quad (6a)$$

The quantity  $-N$  is the signed diattenuation, given by

$$N = -\frac{P_o - P_e}{P_o + P_e}, \quad (6b)$$

where  $P_o$  ( $P_e$ ) is the light power transmitted for light polarized along the ordinary (extraordinary) direction. The quantities  $S$  and  $C$  are given by

$$S = (1 - N^2) \sin (\delta), \quad (6c)$$

$$C = (1 - N^2) \cos (\delta), \quad (6d)$$

where  $\delta$  is the sample retardation, given by

$$\delta = \frac{2\pi d \Delta n}{\lambda}, \quad (6e)$$

where  $d$  is the thickness of the sample,  $\lambda$  is the wavelength of light and  $\Delta n = n_o - n_e$  is the refractive index difference between the ordinary and extraordinary rays. Finally, the direction of the principal axis  $\phi$  and  $C_s = \cos (\phi)$ ;  $S_s = \sin (\phi)$ . As can be seen by comparing Eq. 6a with Eq. 3, the 2-MGE is capable of determining all the relevant parameters for a linear retarder and diattenuator with a single measurement.

### **3. Examples: 2-MGE in reflection**

#### **3.1 Measurement of Optical Functions of Rutile and Anatase (TiO<sub>2</sub>)**

One of the most useful applications of the 2-MGE technique is to determine the optical functions of crystalline uniaxial materials.<sup>9-13</sup> Figure 1 shows the raw data expressed in terms of the  $\rho$  representation for a rutile crystal oriented such that the optic axis was in the plane of the sample, at 45° with respect to the plane of incidence. Similar data is obtained when the optic axis is pointed at -45° with respect to the plane of incidence, but where the signs of the  $s_p$  and  $p_s$  components are changed. This data can

be converted to the optical functions of the material,<sup>9</sup> shown as the complex refractive index ( $n + ik$ ) in Figure 2. When the crystal is transparent, the values of the refractive index are not quite as accurate as the values that can be obtained using minimum deviation methods. However, the values of the complex refractive index in the opaque region are far more accurate than any other technique.

The optical functions of another crystalline form of  $\text{TiO}_2$  (anatase) can also be determined using the 2-MGE, and are also shown in Figure 2. The anatase crystal has quite a different crystal structure, and naturally cleaves such that the optic axis is not in the plane of the sample, but rather makes an angle of  $68.3^\circ$  with the sample surface normal, which can be taken into account in the analysis.<sup>13</sup> Clearly, the complex refractive indices of anatase and rutile are quite different. Below the band edge, rutile has a higher refractive index, as well as a greater value of birefringence, than does anatase. Above the band edge, two critical points are observable in the spectra of anatase, while rutile exhibits one peak.

### 3.2 Measurement of the optical functions of ZnO

Another interesting uniaxial crystalline material is  $\text{ZnO}$ , which has the wurtzite crystal structure, making it optically uniaxial. However, the structure of  $\text{ZnO}$  is very nearly zincblende, which is cubic with isotropic optical properties. Therefore, one would expect there to be a small but measurable birefringence, which is shown in Figure 2, expressed in terms of the complex dielectric function ( $\epsilon = \epsilon_1 + i \epsilon_2 = (n + i k)^2$ ).<sup>10</sup>

Two main features are observable in  $\epsilon_1$  and  $\epsilon_2$  near the direct band edge, and the  $\epsilon_{1e}$ ,  $\epsilon_{2e}$  spectra are nearly the same shape as the  $\epsilon_{1o}$ ,  $\epsilon_{2o}$  spectra --- only shifted up in energy

and up in magnitude. The two features can be identified as the  $n = 1$  and  $n = 2$  excitons associated with a critical point in the joint density of states related to the one-electron band structure. The complex dielectric functions in this region have been successfully fit by Djurisić et. al.<sup>14</sup>

### **3.3 Diffractive Structures**

Structures that show considerable diffraction, such as diffraction gratings can also show strong cross polarization effects. Figure 4 shows experimental 2-MGE data for a ruled diffraction grating blazed to be most efficient at 500 nm. The spectrum depends significantly on the direction of the grating vector, which is the vector perpendicular to the direction of the grooves, but there also is significant symmetry. If the grating vector is at  $0^\circ$ , then there is no cross polarization. However, if the grating vector is placed at  $90^\circ$ , then there is significant cross polarization, contrary to what one would expect for optically uniaxial crystals. Similarly, there is significant symmetry between  $\pm 45^\circ$ , as noted in Figure 4.

## **4. Examples: 2-MGE in transmission**

Clearly, the 2-MGE can also be configured in the transmission mode, where similar parameters are measured, but the meaning is quite different. In our system, two different types of measurements can be performed:<sup>7</sup> First of all, the output from the second polarizer photoelastic modulator pair can be connected to a monochromator, thereby allowing spectroscopic measurements to be made. Secondly, a filter can be used to select a small range of wavelengths, and a lens attached to a x-y stage can be placed such that a small portion of the sample is imaged onto an optical fiber connected to the

photomultiplier detector. By moving the x-y stage, different portions of the sample can be imaged onto the end of the fiber, thereby allowing x-y maps of the sample to be made, although the map is now of parameters such as retardation, diattenuation, and the direction of the principal axis.

#### 4.1 Polaroid

Figure 5 shows the diattenuation  $N$ , as well as the parameters  $S$ , and  $C$  of a Polaroid polarizing film, while the resulting retardation and the direction of the principal axis is shown in Fig. 6.<sup>7</sup> An ideal polarizer will have  $N = -1$ ,  $S = C = 0$ . According to the data in Fig. 5, the Polaroid film is a very good polarizer from  $\sim 520$ - $720$  nm, but deviates significantly from ideality both in the blue and the red parts of the spectrum. Although the diattenuation remains very close to  $-1$  in the blue and the ultraviolet, there is a significant amount of retardation (as indicated by the increased magnitude of  $S$  and  $C$ ). Very little light below  $325$  nm passes through the Polaroid material.

The effects in the red part of the spectrum are particularly dramatic: the magnitude of the diattenuation rapidly drops off, while  $S$  and  $C$  become more important. While the Polaroid is a very good polarizer at  $720$  nm, at  $850$  nm, the Polaroid is more of a retarder than a polarizer. This is quite reasonable, since the matrix material of a Polaroid (polyvinyl alcohol) is often used as a retarder. The amount of retardation (shown in Fig. 5) will depend upon the thickness of the Polaroid, as well as other intrinsic properties of the material. No retardation data is shown between  $\sim 500$  and  $720$  nm, since both  $S$  and  $C$  are small making the retardation measurements very inaccurate.

## 4.2 Lithium Niobate (LiNbO<sub>3</sub>) Under Bias<sup>15</sup>

If a material with a linear or Pockels electro-optic effect is placed in an electric field, then the material may become birefringent. This birefringence is proportional to the applied internal electric field, so the measurement of the electric field-induced birefringence is a direct way to measure internal electric fields. This is critical for several materials that operate under electric field, such as LiNbO<sub>3</sub>, which is used primarily in the electro-optic industry for optical modulators. LiNbO<sub>3</sub> has trigonal symmetry with 3m point group, and is known for an extremely large Pockels effect when the electric field is applied along the z-axis. However, an electric field applied along the x- or y-axes will also induce a birefringence.

Figure 7 shows an x-y map of the retardation and direction of the principal axis of a LiNbO<sub>3</sub> crystal,<sup>15</sup> where the light beam propagates along the z-axis and the electric field is applied along the x-axis. Two sets of x-y maps were obtained. In the first set, labeled AC in Fig. 7, the applied voltage alternated between the positive and negative voltages, staying at the applied voltage for ~0.8 sec. During this time, the 2-MGE measured the retardation and the direction of fast axis, as well as the other parameters. After the other polarity was measured, the lens was moved to obtain similar data at the next x-y point. The second set of measurements, labeled DC in Fig. 7, were taken at a constant bias voltage, and the measurements were not initiated until the sample sat at bias for 10 min.

As can be seen from this plot, the average  $\delta$  of the AC measurements is considerably less than for the DC case, and the distribution of  $\delta$  for the AC case is considerably smoother (smaller standard deviation) than it is for the DC case. For the DC

measurements, there is a build-up of retardation near each contact that is absent in the AC measurements; furthermore, the build-up of retardation on the ground contact for the positive DC measurement is greater, while the negative DC measurement concentrates the retardation on the negative voltage contact. The value of  $\phi$  is  $\sim 138^\circ$  for positive voltages, and  $\sim 45^\circ$  for negative voltages. This value of  $\phi$  does not depend appreciably on whether or not the voltage is ac or dc, but the dc voltage results in a much smaller distribution of  $\phi$ .

A series of time-resolved measurements were performed to examine the time evolution of the retardation and fast axis angle with time. There were at least two components: one or more with a time constant less than our system resolution ( $\sim 50$  ms), and one with a much longer time constant. Figure 8 shows time-resolved measurements of  $\delta$  and  $\phi$  taken near the center of the plots of Fig. 7, with a time resolution of 0.4 sec. After the positive voltage is applied, the retardation increases immediately to 0.153, and then to 0.254 with a time constant of 122 sec. After the voltage is reduced to 0 (grounded), the retardation decreases immediately to 0.113 rad., decaying to its nominal starting value with a time constant of 119.5 sec. Furthermore, the fast axis goes immediately to  $\sim 138^\circ$  upon application of the voltage, and changes very little with time. However, when the contacts are grounded, there is an immediate jump to  $\phi \sim 142^\circ$ , and then a very slow decay in  $\phi$  to its nominal, unbiased value. (Note that the error in  $\phi$  increases considerably with decreasing retardation.)

### 4.3 Cadmium Zinc Telluride (CZT) Under Bias<sup>16</sup>

Another material with considerable potential technological application is cadmium zinc telluride (CZT), which is used for room temperature gamma ray detectors. In order to make a good room temperature gamma detector, it is critical to have the electric field penetrate throughout the entire material. However, most experimental determinations of this are measurements of voltages, which are integrals over the internal electric field. Similar to the case of lithium niobate discussed above, the electric field-induced birefringence can be used to determine the internal electric field in CZT.

The capabilities of the 2-MGE measurement system can be seen in Figure 9, where several x-y maps are shown for a CZT crystal at 0 bias (top), and at +800 V (bottom).<sup>16</sup> In this figure, the ground electrode is at the top edge of the color and the black background interface, and the voltage electrode (either positive or negative) is at the bottom black to color changeover. The x-y maps of 5 different quantities are shown in this figure, all on a linear scale, where the scale is defined at the bottom of the figure. The scales for both measurements are the same, with the exception of the retardation, which is 0-1.2 radians for the +800 V plot, and 0-0.11 radians for the unbiased plot.

As can be seen in Figure 9, the intensity (averaged over the time and expressed in arbitrary units) varies considerably over the x-y map. This variation could come from a number of sources, such as variations in the light intensity from the source itself, variations in the absorption coefficient of the CZT material, or from variations in the surface quality of the CZT crystal. Fortunately, these variations in intensity do not affect the 2-MGE measurements, as long as sufficient light reaches the detector to give

adequate signal-to-noise. The retardation of the unbiased CZT crystal is small but non-zero, and does depend somewhat on the position within the crystal. The direction of the fast axis is  $\sim 90^\circ$ , and does not depend significantly on x-y position. The diattenuation  $N$  also is very small, and the polarization factor  $\beta$  is nearly 1 over most of the x-y plot, except near the voltage contact where it is somewhat low ( $\beta \sim 0.90\text{--}0.95$ ). This indicates that the sample does not significantly depolarize the light beam, except in the region near the voltage contact.

In contrast, the sample under +800 V bias exhibits a strong retardation near the positive electrode (bottom). Moreover, the direction of the fast axis in the region of non-zero retardation approaches  $133^\circ$ , and there is a small but discernable change in the diattenuation. At the edge near the positive voltage electrode, the diattenuation becomes quite large, and there is a clear feature unobservable in any other parameter, possibly indicating a defect in the crystal emanating from this contact (This feature is also observable for lesser positive voltages, although the magnitude of the diattenuation change is somewhat less.). As with the 0-bias case, the polarization factor  $\beta$  is nearly 1 over the most of the x-y mapped region; however, there is a region of decreased  $\beta$  near the positive electrode, which is larger than the similar region for the unbiased measurement. This indicates that light passing near the electrode is partially depolarized in both measurements, but the amount of depolarization is slightly greater for the biased measurement compared to the unbiased measurement. There is very little if any difference in the intensity map between the +800V and 0V bias experiments, showing that the application of the voltage does not affect the intensity.

## 5. Summary

In this paper, we have shown that generalized ellipsometry as implemented using the two-modulator generalized ellipsometer (2-MGE) can be applied to a class of problems inaccessible to standard ellipsometry. The 2-MGE is capable of measuring 8 of the 15 elements of the reduced sample Mueller matrix, which is sufficient for a wide range of applications. Although the 2-MGE can be operated in either the reflection or the transmission modes, the resultant information requires a different interpretation depending upon the mode.

In reflection, the 2-MGE measures the standard ellipsometry parameters, as well as the cross-polarization terms and the depolarization. For single crystal samples, this data can then be used to determine the complex optical functions of the material for both the ordinary and extraordinary directions in the crystal. In the transparent region of the crystal (below the band gap), the information obtained agrees with more accurate minimum deviation methods, but the technique is unsurpassed for the determination of optical functions in the opaque region of the crystal. Several crystals have been measured in this way, and here we have shown the results from two crystal forms of  $\text{TiO}_2$  (rutile and anatase) and  $\text{ZnO}$ . We have also shown that diffractive structures show considerable optical anisotropy when examined using generalized ellipsometry.

The 2-MGE can also be operated in transmission, but the interpretation of the measured parameters is considerably different from reflection measurements. In transmission, the 2-MGE measures sample retardation, diattenuation, circular diattenuation, direction of the principal axis, and the polarization factor. Our instrument

can be configured in two modes: spectroscopic, where the parameters are determined as a function of wavelength, and spatially resolved, where the parameters are determined as a function of position within the crystal. Spectroscopic measurements of a Polaroid revealed that the Polaroid is indeed a good polarizer in the visible, it becomes more of a retarder in the near infrared. Spatially resolved measurements of  $\text{LiNbO}_3$  and CZT revealed that the 2-MGE is capable of measuring the electric field-induced birefringence associated with a penetrating electric field. However, this effect is complicated by the fact that these materials are not simple, and atomic drifting may alter not just the internal electric field, but also the Pockels coefficient.

## **6. Acknowledgements**

The author is indebted to several of his co-workers for their assistance with this work, including C. M. Rouleau, D. E. Holcomb, L. A. Boatner, J. P. Hunn, all of Oak Ridge National Laboratory, A. Burger of Fisk University, and C. O. Griffiths of Hinds Instruments. Research sponsored by the U. S. Department of Energy under contract DE-AC05-00OR22725 with the Oak Ridge National Laboratory, managed by UT-Battelle, LLC.

## References

1. G. E. Jellison, Jr., *Thin Solid Films* **313-314**, 33-39 (1998).
2. G. E. Jellison, Jr. and F. A. Modine, *Appl. Opt.* **36**, 8184-8189 (1997); *ibid*, *Appl. Opt.* **36**, 8190-8198 (1997); *ibid* *Appl. Opt.* **xx**, xxxx-xxxx (2003).
3. M. Schubert, B. Rheinlander, J. A. Woollam, B. Johs, and C. M. Herzinger, *J. Opt. Soc. Am.* **A13**, 875 (1996).
4. M. Schubert, *Thin Solid Films*, **313-314**, 323-332 (1998).
5. H. Yao, J. C. Erikson, L. A. Lam, and R. B. James, *Thin Solid Films*, **313-314**, 351-355 (1998).
6. R. W. Collins, J. Koh, *J. Opt. Soc. Am.*, **A16**, 1997 (1999).
7. G. E. Jellison, Jr., C. O. Griffiths, D. E. Holcomb, and C. M. Rouleau, *Appl. Opt.* **41**, 6555-6566 (2002).
8. C. Brosseau, *Fundamentals of Polarized Light: a Statistical Optics Approach*, (Wiley, New York, 1998).
9. G. E. Jellison, Jr., F. A. Modine, and L. A. Boatner, *Opt. Lett* **22**, 1808-1810 (1997).
10. G. E. Jellison, Jr. and L. A. Boatner, *Phys. Rev. B* **58**, 3586-3589 (1998).
11. G. E. Jellison, Jr., J. O. Ramey, and L. A. Boatner, *Phys. Rev. B* **59**, 9718-9721 (1999).
12. G. E. Jellison, Jr., L. A. Boatner, and C. Chen, *Optical Materials* **15**, 103-109 (2000).
13. G. E. Jellison, Jr., L. A. Boatner, J. D. Budai, B. S. Jeong, and D. P. Norton, *J. Appl. Phys.* **93**, 9537-9542 (2003).
14. A. B. Djuricic, Y. Chan, and E. H. Li, *Appl. Phys. A* **76**, 37 (2003).
15. G. E. Jellison, Jr., C. O. Griffiths, and D. E. Holcomb, *Appl. Phys. Lett.* **81**, 1222-1224 (2002)
16. G. E. Jellison, Jr., D. E. Holcomb, C. O. Griffiths, M. Grozas, A. Burger, L. Li, and F. Yu, *J. Elect. Mat.* **XXX**, xxx-xxx (2003). Accepted for publication.

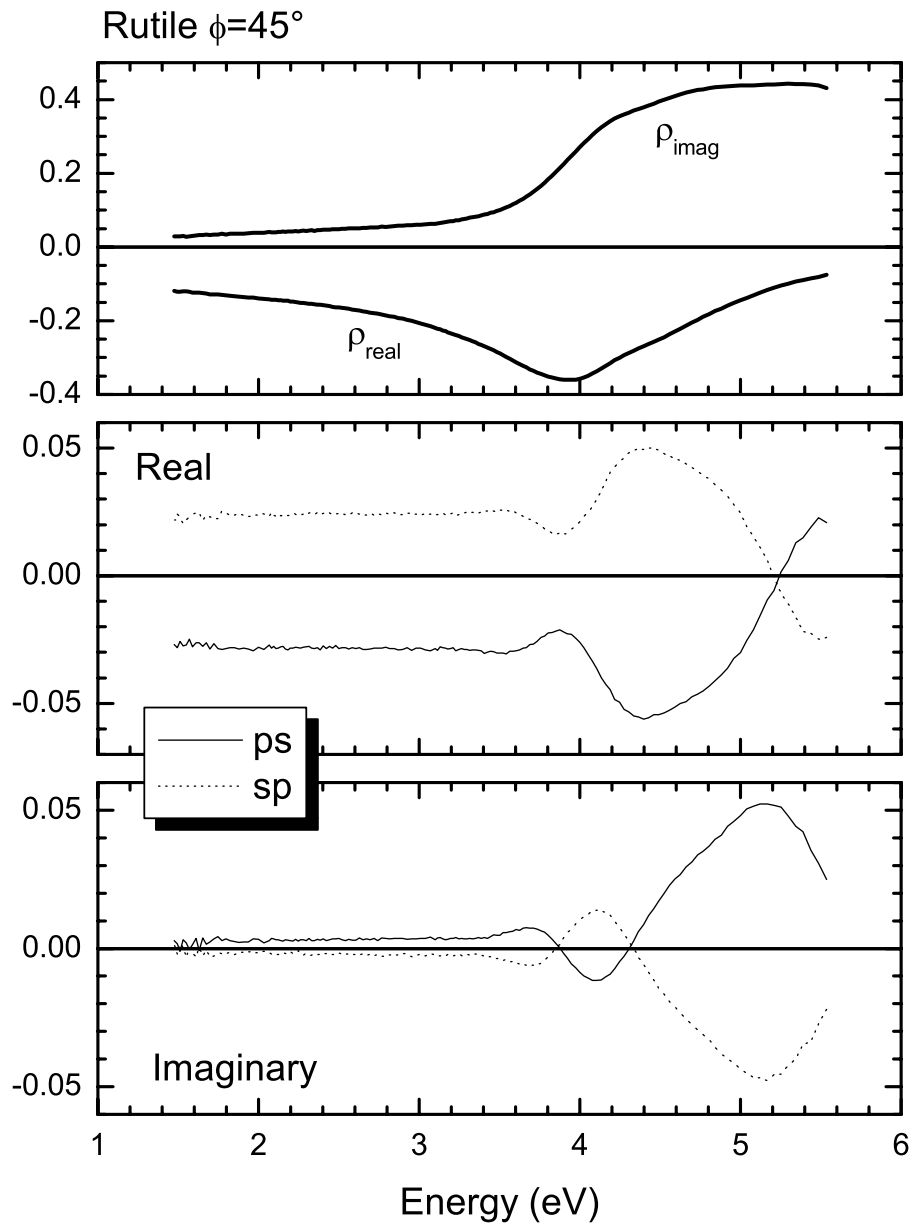


Figure 1. The spectroscopic values of  $\rho$  determined using 2-MGE for Rutile where the direction of the optical axis was in the plane of the sample, oriented at  $45^\circ$  with respect to the plane of incidence

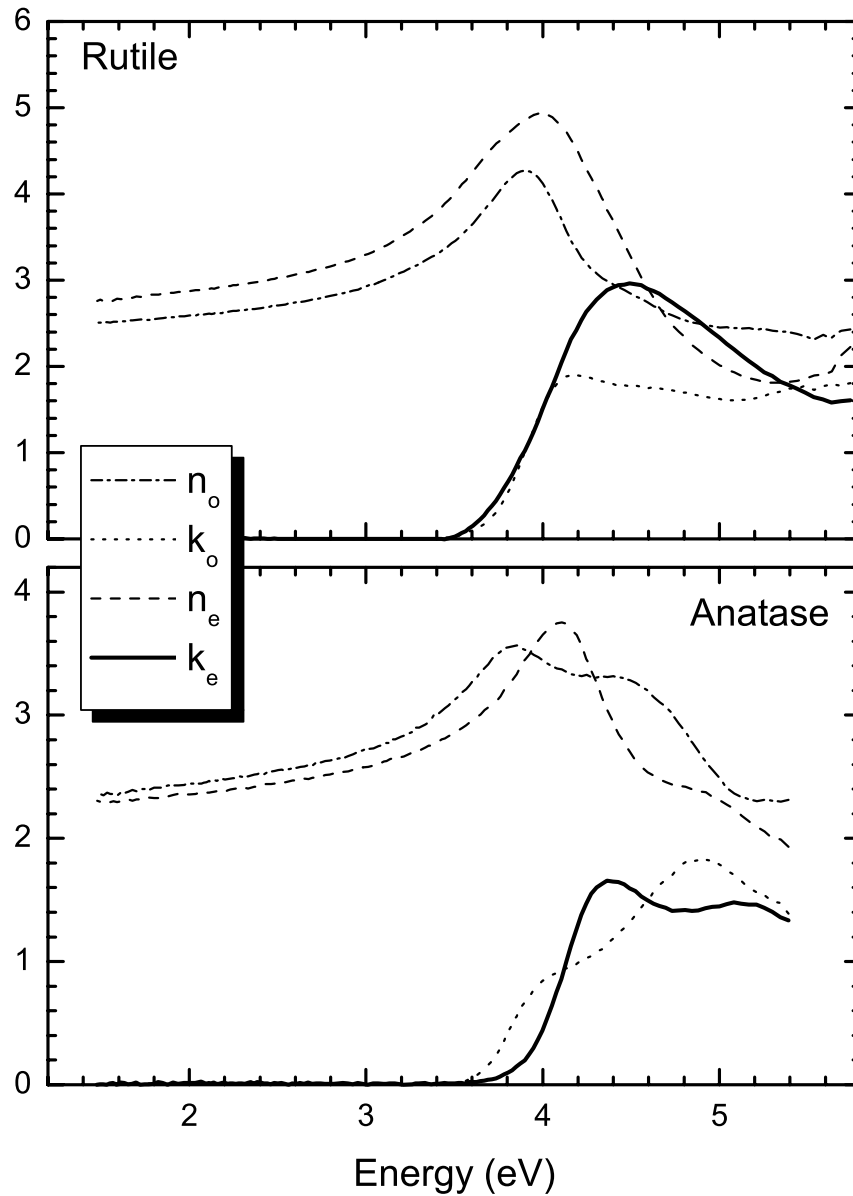


Figure 2. The spectroscopic values of the ordinary (o) and extraordinary (e) refractive index  $n$  and the extinction coefficient  $k$  for rutile and anatase. The values of  $n$  and  $k$  were determined from the data shown in Figure 1 for rutile, while the original data for anatase is not shown.

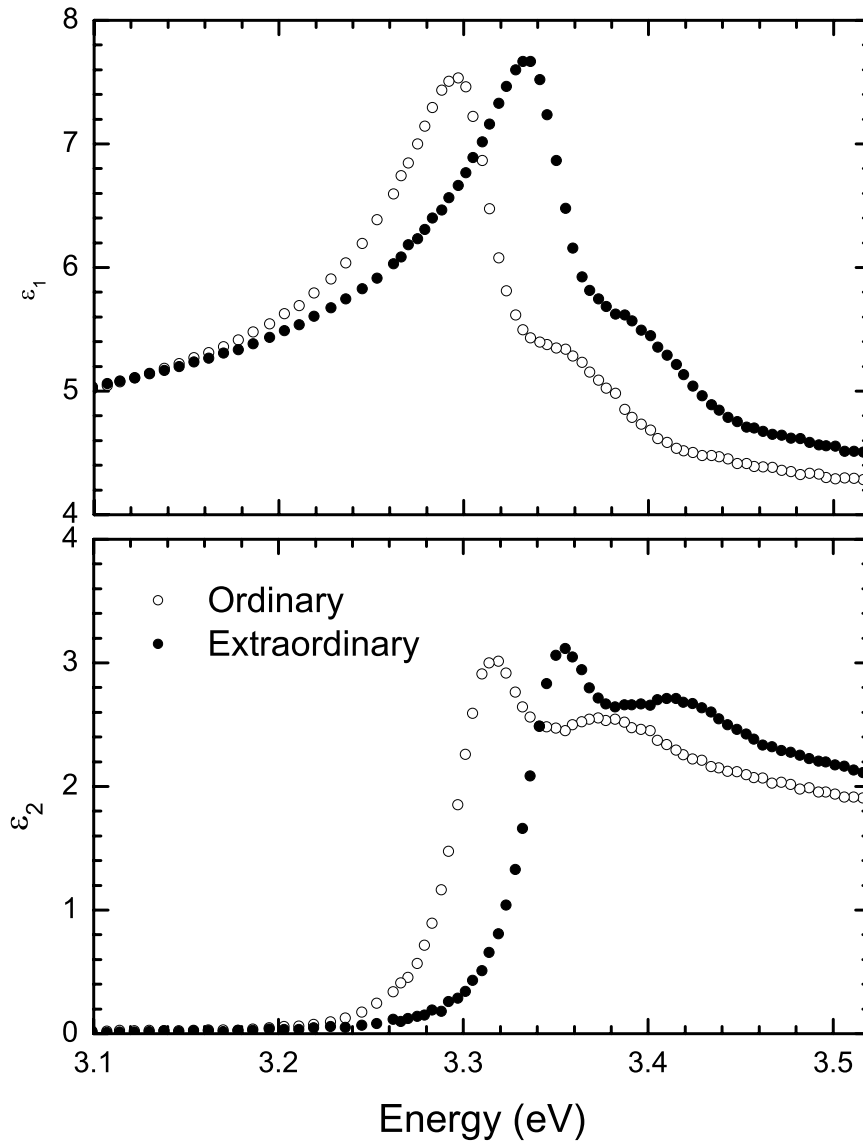


Figure 3. The spectroscopic values of the complex dielectric function for ZnO near the direct transition.

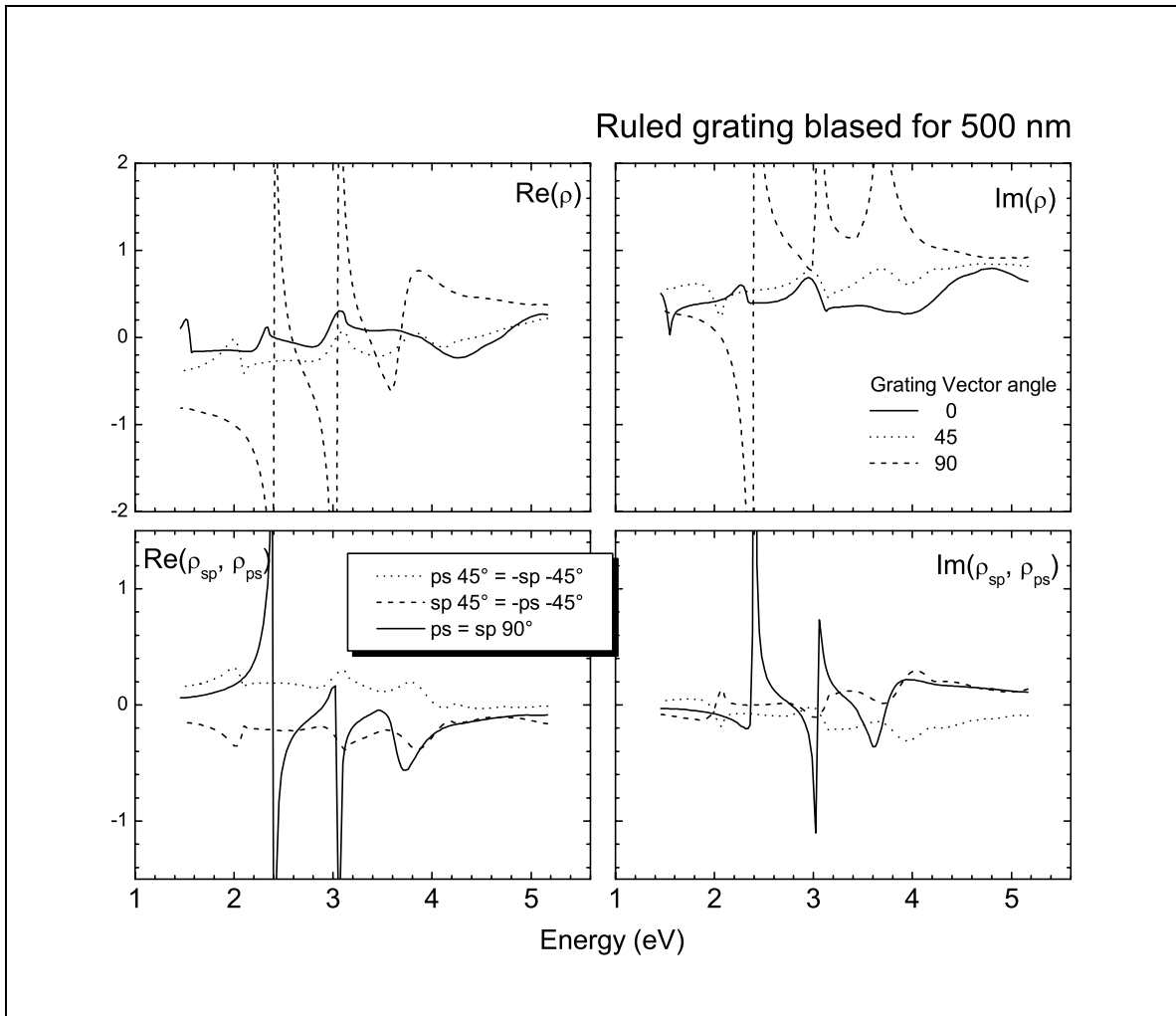


Figure 4. The spectroscopic values of the complex  $\rho$  as measured from a replica ruled diffraction grating blazed for optimum performance at 500 nm. The angle listed is the grating vector, which is perpendicular to the grooves.

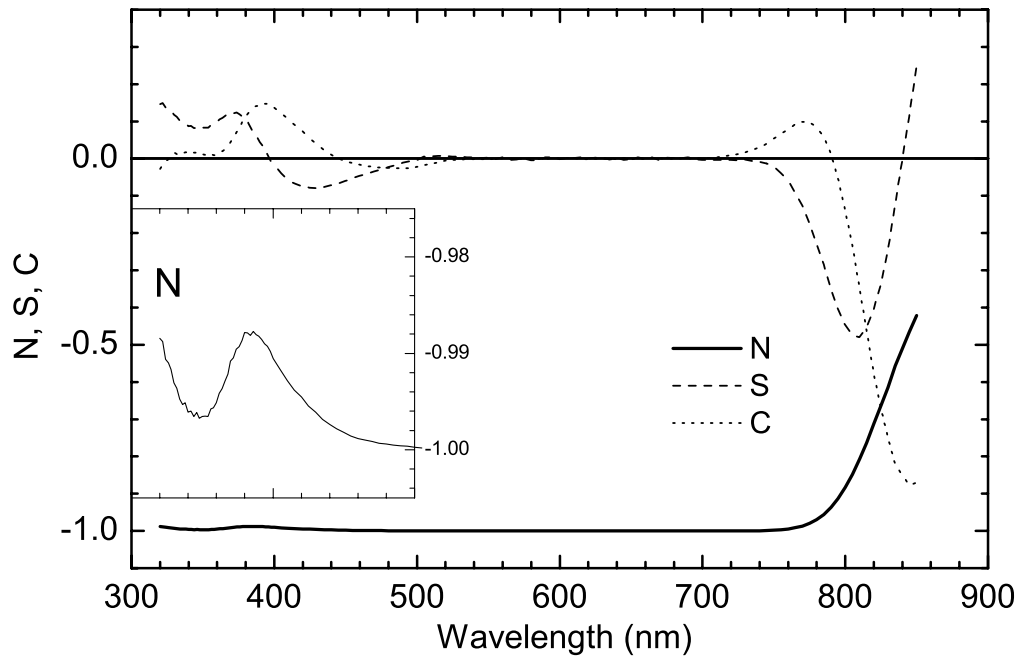


Figure 5 The spectroscopic values of N, S, and C for transmission through a Polaroid.

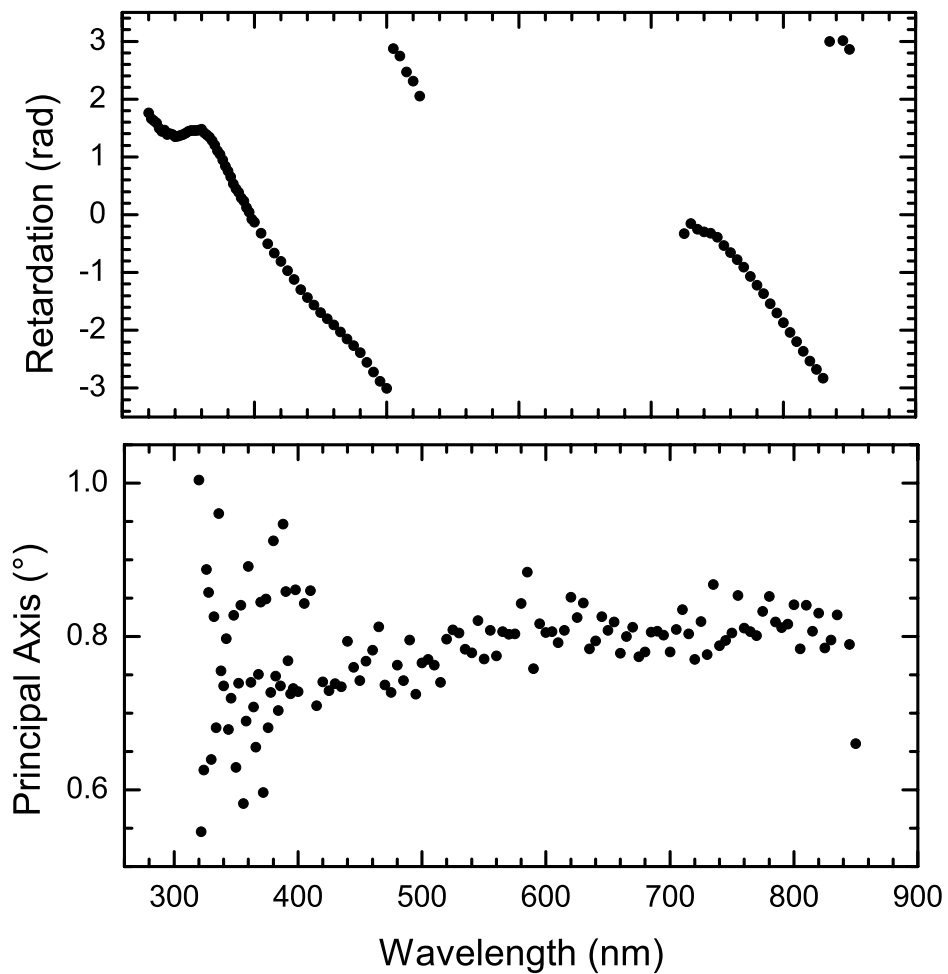


Figure 6. The calculated values of the retardation and the direction of the principal axis versus the wavelength, determined from the data shown in Figure 1.

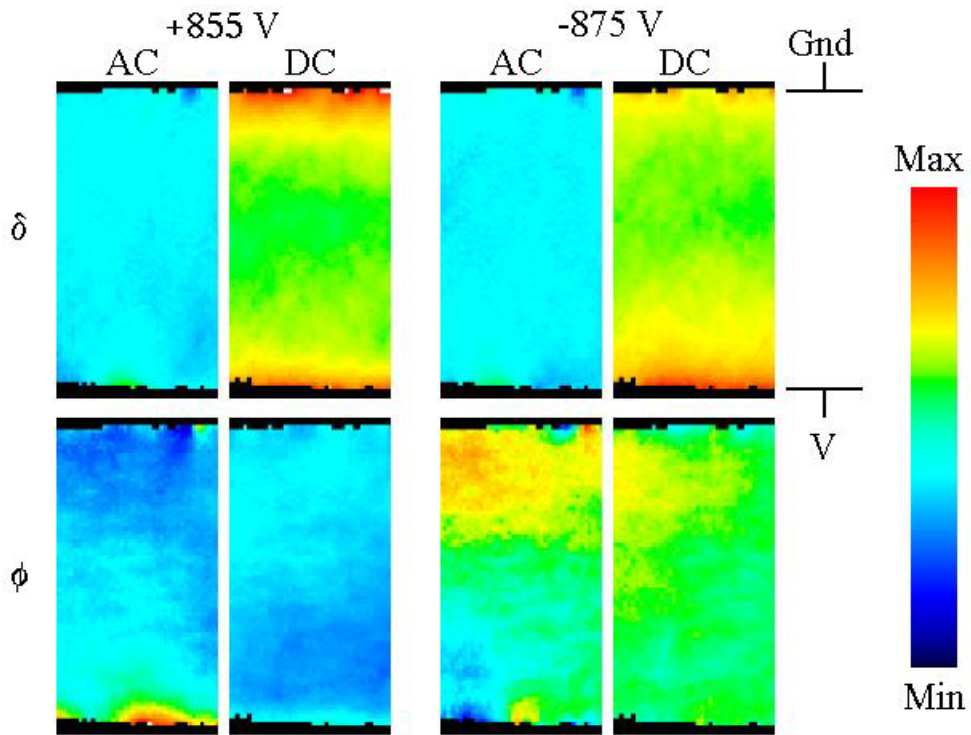


Figure 7. An x-y color plot of the retardation  $\delta$  and fast axis angle  $\phi$  as a function of applied voltage. The retardation scale (min to max) is 0-0.4 rad, while the Fast axis angle range is  $25^\circ$ - $55^\circ$  for negative voltages and  $125^\circ$ - $160^\circ$  for positive voltages. The horizontal (x) dimension is 1.27 mm (41 pixels) and the vertical (y) dimension is 2.45 mm (79 pixels). The AC measurements were made by alternating between the positive and negative values, dwelling at each voltage for  $\sim 0.8$  sec. The DC measurements were made by putting the sample at voltage for  $\sim 10$  min before beginning measurements..

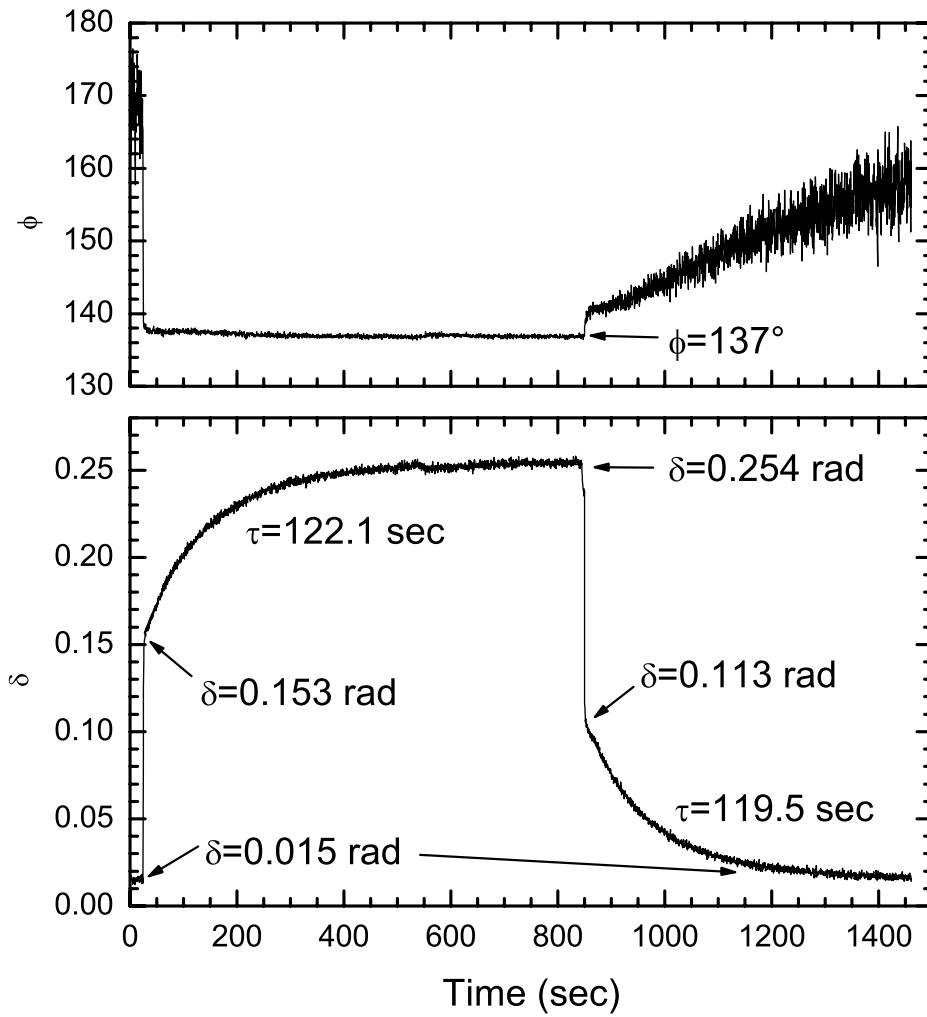


Figure 8. A plot of the retardation and fast axis angle as a function of time at a single point near the center of the field shown in Fig.7.

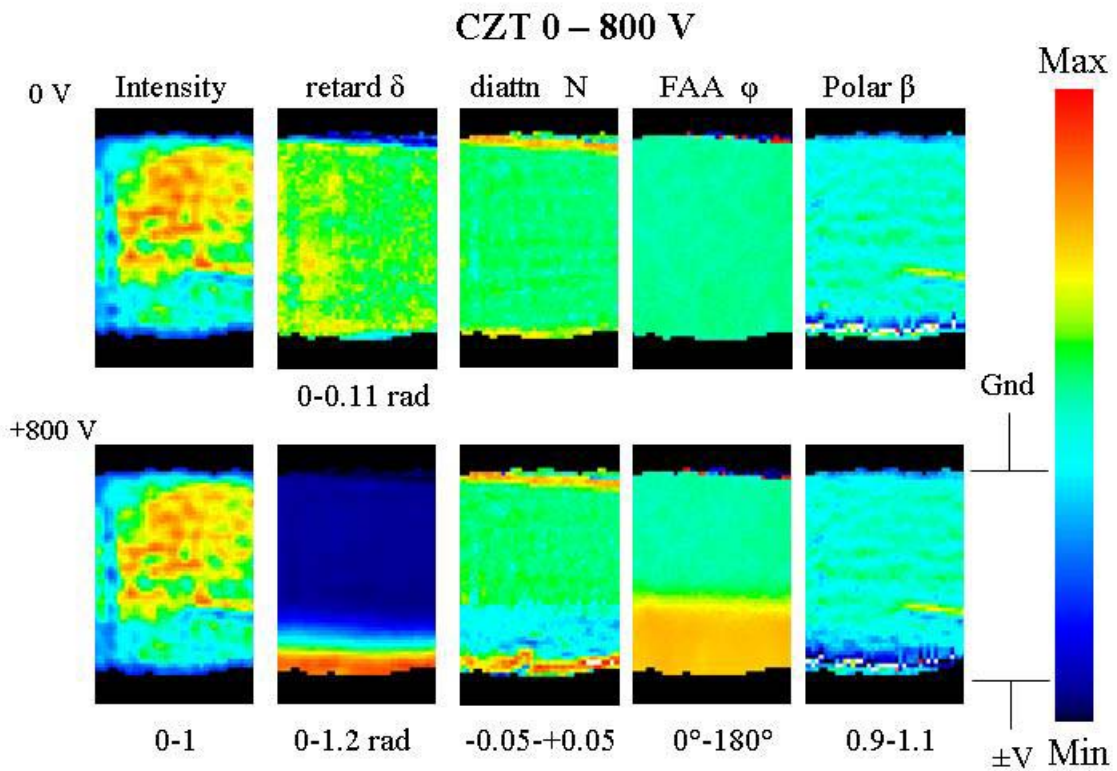


Figure 9. x-y maps of several parameters of a CZT sample unbiased (top) and under +800 V bias (bottom). The ground electrode is at the top black-color interface of each figure, while the bias contact is at the bottom to black-color interface. The color scale is defined at the right, where the maximum and minimum values are given at the bottom of the figure. The color scales for the intensity, N,  $\phi$ , and  $\beta$  are the same for both biases, but are different for the retardation  $\delta$